



## Quantification of NO<sub>x</sub> uptake in plain and TiO<sub>2</sub>-doped cementitious materials



Q. Jin<sup>a</sup>, E.M. Saad<sup>b</sup>, W. Zhang<sup>a</sup>, Y. Tang<sup>a,b</sup>, K.E. Kurtis<sup>a,\*</sup>

<sup>a</sup> School of Civil and Environmental Engineering, Georgia Institute of Technology, Atlanta, GA, USA

<sup>b</sup> School of Earth and Atmospheric Sciences, Georgia Institute of Technology, Atlanta, GA, USA

### ARTICLE INFO

#### Keywords:

TiO<sub>2</sub>  
NO<sub>x</sub> photodegradation  
Cement  
Microstructure  
Nitrite/Nitrate

### ABSTRACT

This study brings new understanding of the interaction of nitrogen oxides (NO<sub>x</sub>) with cement-based materials, necessary for optimizing these materials for NO<sub>x</sub> sequestration. The masses of nitrites and nitrates produced through NO<sub>x</sub> uptake in cement-based materials are quantified for both plain portland cement pastes (OPC) and nano TiO<sub>2</sub>-doped OPC. Both nitrite and nitrate were bound within plain OPC, with a nitrite:nitrate ratio of 1:2. This intrinsic NO<sub>x</sub> sequestration capacity is attributed to the microstructural features and alkalinity of cement-based materials. The capacity is increased by 360%, with a lower nitrite:nitrate ratio of 1:1.3, in TiO<sub>2</sub>-doped OPC. The increase in NO<sub>x</sub> uptake and the change in nitrite:nitrate ratio is attributed to the microstructural differences and activation of photocatalytic reactions that are associated with TiO<sub>2</sub> addition. Comparing NO<sub>x</sub> exposure with and without UV on TiO<sub>2</sub>-doped OPC shows that photocatalytic activities have greater influences on NO<sub>x</sub> uptake than microstructural differences induced by TiO<sub>2</sub> addition.

### 1. Introduction

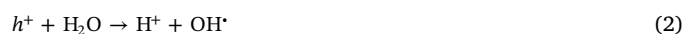
Nitrogen oxide (NO<sub>x</sub>) emission is one of the most hazardous air pollutants, causing a variety of health problems such as respiratory system impairment and vision problems. NO<sub>x</sub> also contributes to global warming, acid rain, ground-level smog, and decreased water quality [1,2]. The two most common forms of NO<sub>x</sub> in the troposphere are nitric oxide (NO) and nitrogen dioxide (NO<sub>2</sub>). NO is directly emitted from high temperature combustion, in particular from combustion engines in motor vehicles. NO<sub>2</sub> is produced from the interaction of NO with ozone or molecular oxygen [3,4]. Decades-long efforts to reduce NO<sub>x</sub> levels have been mainly devoted to environmental legislation, improvements in combustion efficiency, and technologies to reduce post-combustion NO<sub>x</sub> [5,6].

Among different technologies for reducing atmospheric NO<sub>x</sub>, titanium dioxide (TiO<sub>2</sub>) photocatalysts [7,8] have been of great interest. Since concrete is a widely used material globally, substantial efforts have been dedicated toward understanding its potential roles in NO<sub>x</sub> binding through the introduction of photocatalysts. For example, paving with concrete containing or coated with TiO<sub>2</sub> nanoparticle photocatalysts [9,10] has been shown to reduce the amount of motor vehicle emission-derived NO<sub>x</sub> in the air [11–13]. Given the ubiquity of concrete infrastructure, interest in expanding the applications of cement-based materials, such as to concrete bridges and buildings, is

growing.

Previous research has mainly focused on the manner of photocatalyst addition (i.e., interblended vs. coatings) and their percent addition in cementitious substrates [14–16]. In these applications, both anatase and rutile TiO<sub>2</sub> nanoparticles have been shown to effectively remove NO<sub>x</sub> from the atmosphere in the presence of water, oxygen, and UV light [17,18]. Studies have investigated the effects of microstructure and surface features on the photocatalytic performance of TiO<sub>2</sub> nanoparticles blended cementitious materials [19,20]. Studies also examine the effects of mixing and operation conditions on photocatalytic efficiency [21–23], and the feasibility of using alternative cementitious materials in combination with TiO<sub>2</sub> nanoparticles [24,25]. Yet, despite the considerable efforts in the above areas, a fundamental understanding of the speciation and fate of sequestered NO<sub>x</sub> in the cementitious materials remains elusive.

In general, photocatalysis is believed to result in the oxidation of NO<sub>x</sub> by hydroxyl radicals (OH·) and superoxide radicals (O<sub>2</sub>·<sup>-</sup>). This leads to the formation of nitrite (NO<sub>2</sub><sup>-</sup>) and/or nitrate (NO<sub>3</sub><sup>-</sup>) through a series of photocatalytic oxidation reactions [26–30], which can be generalized through the following equations:



\* Corresponding author.

E-mail address: [kkurtis@gatech.edu](mailto:kkurtis@gatech.edu) (K.E. Kurtis).



However, the relative abundance of the produced nitrite and/or nitrate has not been clearly defined, and likely depends on the characteristics of the substrate material.

Because cement-based materials are structurally and chemically complex hydrated materials, they may influence and participate in these photocatalytic reactions, such as affecting the amount of nitrite and/or nitrate formed and the manner in which  $NO_x$  is bound within the material. Such information on N speciation and mass distribution is important for a number of reasons. First, due to the intrinsic chemical differences between nitrite and nitrate, they can interact differently with cementitious phases. For example, these ions could dissolve in the alkaline pore solution [31], adsorb to hydrate surfaces [31], and/or to substitute for sulfate ions within aluminum-bearing hydrated phases (AFm and AFt) [32]. Second, nitrite and nitrate, when incorporated into steel-reinforced concrete, can serve as corrosion inhibitors, with nitrates considered to be better inhibitors [33]. Recent studies have also shown that adjusting nitrite and nitrate concentrations to achieve a desirable ratio with chloride concentrations can enhance the corrosion resistance [34]. Therefore, information about the concentration and relative percentages of nitrite and nitrate formation is critical to understanding their interactions with the complex cementitious materials and to designing these materials for maximized  $NO_x$  uptake and corrosion resistance.

To quantify the concentration and relative percentages of nitrite and nitrate in  $TiO_2$ -doped cementitious materials after  $NO_x$  exposure, this study employs a novel experimental method combining wet chemical extraction, ultraviolet-visible (UV-vis) spectrophotometry, and ion chromatography (IC) measurements. While these approaches have been widely used in determining nitrite and nitrate concentration in other systems [35,36], this is the first time that these approaches have been used in cement-based materials. The  $NO_x$  sequestration capacity of various cementitious materials is determined through the measured nitrite and nitrate concentrations. The mass balance between the  $NO_x$  input and  $NO_x$  measured at the outlet is compared to measured nitrite and nitrate quantities in the exposed cement paste. Microstructural analysis is also carried out in this study to establish a relationship between microstructural features of cement-based materials with  $NO_x$  uptake.

## 2. Experiments and methods

### 2.1. Materials

The samples were prepared from ASTM C150 Type I/II ordinary portland cement (OPC, Argos, Atlanta, Georgia, USA), combined with 5 wt%  $TiO_2$  (KRONOClean® 7050, Kronos Worldwide). The water-to-solid ratio was kept constant at 0.40. The chemical composition of the cement was obtained by oxide analysis (ASTM C114 [37]) and used to determine the Bogue composition (Table 1). The characteristics of the  $TiO_2$  are listed in Table 2.

**Table 1**  
Composition (wt%) and loss on ignition (LOI) of the cement.

| C <sub>3</sub> S | C <sub>2</sub> S | C <sub>3</sub> A | C <sub>4</sub> AF | SiO <sub>2</sub> | Al <sub>2</sub> O <sub>3</sub> | Fe <sub>2</sub> O <sub>3</sub> | CaO  | MgO | SO <sub>3</sub> | Na <sub>2</sub> O | LOI |
|------------------|------------------|------------------|-------------------|------------------|--------------------------------|--------------------------------|------|-----|-----------------|-------------------|-----|
| 62.9             | 7.6              | 6.9              | 9.2               | 19.2             | 4.5                            | 3                              | 62.8 | 3.6 | 3.1             | 0.5               | 2.6 |

**Table 2**  
Characteristics of  $TiO_2$  photocatalyst (provided by manufacturer).

| $TiO_2$ content | Phase   | Density               | Bulk density | Specific surface area   |
|-----------------|---------|-----------------------|--------------|-------------------------|
| > 85%           | Anatase | 3.9 g/cm <sup>3</sup> | 300 g/L      | > 225 m <sup>2</sup> /g |

To increase the surface area and the reaction potential between  $NO_x$  and the cementitious materials, crushed samples were produced from a cementitious plate. The plate was cast by first adding  $TiO_2$  to deionized water (18.2 mΩ-cm) and mixing for 1 min using a handheld electric mixer to facilitate dispersion [31]. Then cement was added to the  $TiO_2$  suspension and mixed for an additional 2 min. Cementitious plates were cast in plastic molds with dimension of 50.8 mm × 50.8 mm × 9.5 mm (width × length × height) and stored at 23 ± 2 °C under polyethylene sheeting to maintain a high humidity. After 24 h, the plates were removed from the molds and subsequently cured in limewater at room temperature (23 ± 2 °C) for 28 days. After curing, the plates were conditioned at 23 ± 2 °C and 50 ± 5% relative humidity until reaching constant mass (i.e., < 0.5 wt% change over a 6-h period). The crushed samples were obtained by hand crushing the conditioned plate and sieving to obtain particles which passed the No.18 (1 mm) and were retained on the No. 30 (0.6 mm) sieves. Samples were stored in double sealed plastic bags prior to the microstructural analysis and  $NO_x$  photodegradation tests to avoid drying or carbonation.

### 2.2. Microstructural analysis

The specific surface area (SSA) and pore size distribution of the crushed samples, prior to  $NO_x$  exposure, were determined by  $N_2$  adsorption and desorption. Approximately 2 g of each sample were analyzed in a specific surface area gas analyzer (Micromeritics ASAP 2420) over a relative pressure range of 0.01 to 0.99. The crushed samples were degassed at 10 μmHg pressure for 12 h prior to the analysis. The SSA was determined by Brunauer–Emmett–Teller (BET) theory [38] using  $N_2$  adsorption isotherm performed over a relative pressure range of 0.05 to 0.30. The pore size distribution was determined using Barrett, Joyner and Halenda (BJH) method [39] on the data obtained from the desorption isotherm [40].

Although it has been noted that surface area measurements vary with technique, adsorbate, and sample preparation [41], the variation due to the sample preparation was minimized in this study by using a consistent experimental method and procedure, as described above, facilitating comparison among samples. In addition, the  $N_2$  adsorption and desorption technique for obtaining SSA and pore size distribution has been commonly used for cementitious materials and can ensure semiquantitative comparisons of different cementitious materials [42].

### 2.3. $NO_x$ photodegradation

A schematic illustration of the  $NO_x$  photodegradation test setup is shown in Fig. 1. The test was performed following procedures in ISO 22197 [43] and JIS R 1701 Standards [44]. Two grams (2.00 ± 0.01 g) of samples were placed in a borosilicate photoreactor, with both ends sealed with a filter and screw cap. As recommended by the aforementioned standards, the  $NO_x$  gas used in this study was prepared by mixing 1000 ppb nitric oxide gas in ultrapure dry air and passed through the reactor at a constant flow rate of 1 L/min. For the purpose of consistency, the  $NO_x$  in this study refers to this particular mixed gas. The reaction was conducted at 23 ± 2 °C and 50 ± 5% relative humidity. The sample-loaded reactor was placed under two 40 W UV fluorescent lamps (Damar Worldwide) with peak emission at 365 nm. The UV light intensity at the sample surface was maintained at 10 W/m<sup>2</sup> by adjusting the distance between the UV light source and the samples, which reside on the bottom surface of the photoreactor. The initial gas concentration was kept at 1000 ppb before turning on the UV light. Once the gas

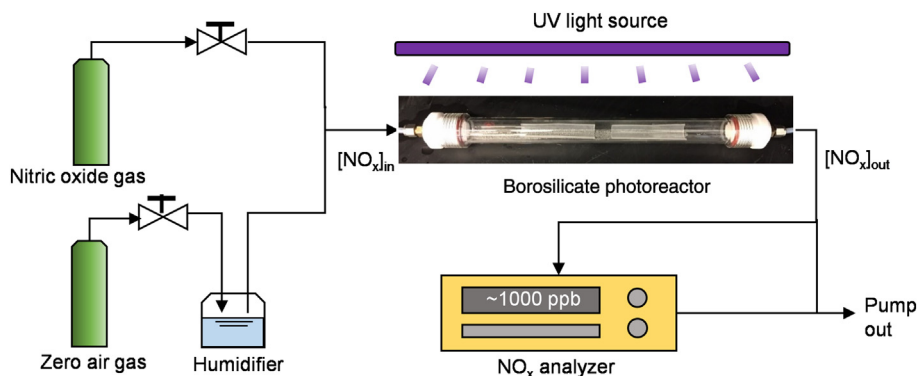


Fig. 1. Experimental setup for NO<sub>x</sub> photocatalytic degradation test.

concentration stabilized (1 h stabilization time), the UV light exposure started and continued for 5 h. After the UV light was turned off, the gas concentration was allowed to re-stabilize for another hour. The gas concentration throughout the experiment was measured by a chemiluminescent NO/NO<sub>2</sub>/NO<sub>x</sub> analyzer (Model 200A, Teledyne API). The entire test setup was covered by a black light-blocking canvas to prevent ambient light from affecting the reaction.

#### 2.4. Sample matrix

Six groups of experiments were conducted in triplicate, with varied sample composition and reaction conditions. Sample labels, test matrix, material composition, and exposure conditions are summarized in Table 3. Samples PB, PB-N and PB-N-V were control groups prepared with plain OPC (i.e., no TiO<sub>2</sub> doping), and Samples PT, PT-N and PT-N-V contained 5% TiO<sub>2</sub> by weight of OPC. As outlined in Table 3, both doped and un-doped samples were subjected to three exposure conditions: 1) without NO<sub>x</sub> or UV exposure; 2) with NO<sub>x</sub> but without UV exposure; and 3) with both NO<sub>x</sub> and UV exposures. The samples subjected to Condition 3 were exposed to NO<sub>x</sub> and UV for 5 h, plus one-hour stabilization time at beginning and another hour for re-stabilization time at the end (see Section 2.3 for detailed exposure arrangement). The samples subjected to Condition 2 were exposed to NO<sub>x</sub> for a total of seven-hour period without UV (same period of NO<sub>x</sub> exposure as Condition 3). These exposure conditions and arrangements were selected to examine the individual and combined effects of NO<sub>x</sub> exposure, UV exposure, and TiO<sub>2</sub> doping. At the end of each experiment, the samples were removed from the reactor and subjected to chemical extraction and nitrite and nitrate measurements within 24 h.

Table 3

Summary on the test matrix, material composition, exposure conditions, and measured concentration of nitrogen in the forms of nitrite and nitrate.

| Group ID <sup>a</sup> | OPC | 5% TiO <sub>2</sub> | Exposure Condition |    | Mass of Nitrogen (mg/kg) |                   |
|-----------------------|-----|---------------------|--------------------|----|--------------------------|-------------------|
|                       |     |                     | NO <sub>x</sub>    | UV | Nitrite detection        | Nitrate detection |
| PB                    | ×   |                     |                    |    | BDL                      | BDL               |
| PB-N                  | ×   |                     | ×                  |    | 2.77 ± 0.09              | 5.83 ± 0.55       |
| PB-N-V                | ×   |                     | ×                  | ×  | 2.78 ± 0.02              | 5.66 ± 0.45       |
| PT                    | ×   | ×                   |                    |    | BDL                      | BDL               |
| PT-N                  | ×   | ×                   | ×                  |    | 5.80 ± 0.22              | 8.08 ± 1.77       |
| PT-N-V                | ×   | ×                   | ×                  | ×  | 16.99 ± 0.35             | 22.26 ± 3.25      |

<sup>a</sup> Sample ID: P – OPC, B – plain cement pastes without TiO<sub>2</sub>, T- 5% TiO<sub>2</sub> inclusion, N – samples under NO<sub>x</sub> exposure, and V – samples under UV radiation. For example, PT-N-V indicates TiO<sub>2</sub>-doped OPC samples that are exposed to both NO<sub>x</sub> gas and UV light; BDL: below detection limit.

#### 2.5. Nitrite and nitrate measurements

The recovered samples were suspended in anoxic deionized (DI) water (purged by N<sub>2</sub> gas) in amber bottles to prevent further photo-induced reactions. Preliminary tests were conducted to determine the appropriate solid:liquid ratio (0.1 g in 10 to 100 mL), extraction time (4 h to 1 week), and solvent (DI water or KCl solution). A solid:liquid ratio of 0.1 g in 40 mL DI water, and 48 h reaction time were selected for all experiments. Varying these parameters to facilitate extraction – such as increasing dilution, increasing reaction time – produced no measurable increase in nitrite and nitrate concentration, demonstrating the suitability of this method for full extraction. After the extraction, the suspension was filtered through a 0.45 μm syringe filter. The pH of the filtrate was measured by pH test strips (EMD chemicals) and was found to be around 10. The filtrate was then analyzed for both nitrite and nitrate concentrations.

Nitrite concentration was determined using a colorimetric assay kit (Roche, Sigma Aldrich) and measured at 540 nm on a UV–vis spectrometer (Cary 60, Agilent). Nitrate concentration was determined using ion chromatography (IC, Dionex). The IC is equipped with an Ionpac® AS14A column (4 × 250 mm) combined with an Ionpac® AG14A guard column (4 × 50 mm), and a Dionex ED40 electrochemical detector. The mobile phase contained 8 mM Na<sub>2</sub>CO<sub>3</sub> and 1 mM NaHCO<sub>3</sub>, and the flow rate was 0.8 mL/min.

#### 2.6. Examination of NO<sub>x</sub> uptake and nitrite/nitrate formation

The nitrogen (N) mass of NO<sub>x</sub> uptake ( $m_N$ ) from the photo-degradation test was compared with the total N mass from the nitrite ( $m_N'$ ) and nitrate ( $m_N''$ ) measurements. The total amount of NO<sub>x</sub> uptake throughout the photocatalytic process can be determined by Eqs. (9)–(11). For the purpose of comparison, the specific NO<sub>x</sub> uptake (normalized by sample mass) is used in this study and with a unit of mg N per kg solid (denoted as mg/kg for simplicity).

$$Q_N = \frac{f}{V} \int_0^T (C_{[NO_x]_{uptake}}) dt \quad (9)$$

$$C_{[NO_x]_{uptake}} = C_{[NO_x]_{in}} - C_{[NO_x]_{out}} \quad (10)$$

$$m_N = Q_N \times M_N \quad (11)$$

where  $Q_N$  = the amount of N uptake that is measured by NO<sub>x</sub> analyzer (mol),  $C_{[NO_x]_{uptake}}$  = uptake concentration of NO<sub>x</sub> (ppb),  $C_{[NO_x]_{in}}$  = inlet concentration of NO<sub>x</sub> (ppb),  $C_{[NO_x]_{out}}$  = outlet concentration of NO<sub>x</sub> (ppb),  $t$  = time of NO<sub>x</sub> absorption (min),  $T$  = the duration of the photocatalytic process (300 min),  $f$  = flow rate of NO<sub>x</sub> at 23 °C and 1.01 kPa (L/min),  $V$  = 24.3 L (the volume of 1 mol ideal gas at 23 °C and 1.01 kPa),  $m_N$  = the mass of N uptake (mg/kg), and  $M_N$  = the molar mass of N = 14 g/mol.

The N mass from nitrite and nitrate measurements is determined by

Eqs. (12)–(15):

$$m_{NO_2^-} = C_{NO_2^-} \times DF \tag{12}$$

$$m_{NO_3^-} = C_{NO_3^-} \times DF \tag{13}$$

$$m'_N = m_{NO_2^-} \times \frac{M_N}{M_{NO_2^-}} \tag{14}$$

$$m''_N = m_{NO_3^-} \times \frac{M_N}{M_{NO_3^-}} \tag{15}$$

where  $m_{NO_2^-}$  = the mass of nitrite (mg/kg),  $m_{NO_3^-}$  = the mass of nitrate (mg/kg),  $C_{NO_2^-}$  = the concentration of nitrite measured by UV-vis (ppm),  $C_{NO_3^-}$  = the concentration of nitrate measured by IC (ppm), DF = dilution factor used for wet chemical extraction (400 for all samples),  $m'_N$  = the mass of nitrogen from nitrite (mg/kg),  $m''_N$  = the mass of nitrogen from nitrate (mg/kg),  $M_{NO_2^-}$  = the molar mass of nitrite = 46 g/mol, and  $M_{NO_3^-}$  = the molar mass of nitrate = 62 g/mol.

### 3. Results and discussion

#### 3.1. Microstructure

The measured specific surface area (SSA) was  $10.23 \pm 0.98 \text{ m}^2/\text{g}$  for the plain OPC samples (PB) and  $16.90 \pm 0.06 \text{ m}^2/\text{g}$  for the  $\text{TiO}_2$ -doped OPC samples (PT) after 28 days of hydration. The SSA is increased by 65% due to the  $\text{TiO}_2$  addition. The pore size distribution profiles of the PB and PT samples (Fig. 2) show larger amount of very small pores (< 5 nm) in Sample PT. The higher SSA and greater amount of micropores are attributed to the inclusion of  $\text{TiO}_2$  nanoparticles, which possess intrinsically high SSA and ability to accelerate alite ( $\text{C}_3\text{S}$ ) hydration due to nucleation and growth effects [45,46]. The surface area of C-S-H is in the range of 10s to 100s of  $\text{m}^2/\text{g}$  [47] and that of  $\text{TiO}_2$  nanoparticles is larger than  $225 \text{ m}^2/\text{g}$  (Table 2). Therefore, while it is difficult to discern between the physical and chemical effects of nanoparticle addition, it is clear that  $\text{TiO}_2$  addition leads to a higher SSA and larger amount of micropores in hydrated cementitious materials. The relationship between the microstructural property and  $\text{NO}_x$  uptake will be further discussed in Section 3.3.1.

#### 3.2. Mass balance of $\text{NO}_x$ uptake and nitrite/nitrate formation

The result of the  $\text{NO}_x$  photodegradation test during the UV-irradiation period for Sample PT-N-V ( $\text{TiO}_2$ -doped OPC exposed to both  $\text{NO}_x$  and UV) is shown in Fig. 3, where an instantaneous drop of  $\text{NO}_x$  concentration occurred upon UV illumination. This photodegradation of  $\text{NO}_x$  continued throughout the 5 h test period, but at a decreasing

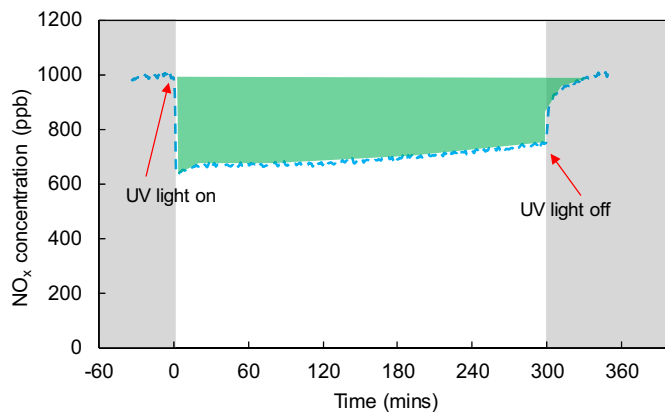


Fig. 3. Photodegradation of  $\text{TiO}_2$ -doped OPC sample (PT-N-V) that are exposed to both  $\text{NO}_x$  and UV light.

rate. This phenomenon agrees with findings by other researchers [10,12,21]. When the UV light was turned off,  $\text{NO}_x$  concentration returned to the initial value. The total N mass of  $\text{NO}_x$  uptake ( $m_N$ ) is denoted by the shaded region in Fig. 3 and calculated to be  $25.82 \pm 0.57 \text{ mg/kg}$ .

The N masses from nitrite and nitrate measurements are listed in Table 3. The N mass of nitrite and nitrate formation due to photocatalytic reactions can be estimated by the difference between Sample PT-N and PT-N-V. The N mass present in nitrite form ( $m'_N$ ) is  $11.20 \pm 0.42 \text{ mg/kg}$  and in nitrate form ( $m''_N$ ) is  $14.18 \pm 3.70 \text{ mg/kg}$ . The total N mass in nitrite and nitrate combined ( $m'_N + m''_N$ ) is  $25.38 \pm 3.73 \text{ mg/kg}$ . Therefore, a mass balance is achieved with total N mass in  $\text{NO}_x$  uptake during the photocatalytic process falling within the margin of error for the total N mass presented in nitrite and nitrate ( $m_N \cong m'_N + m''_N$ ).

#### 3.3. $\text{NO}_x$ uptake

The  $\text{NO}_x$  uptake by cement-based materials can be considered to occur via a two-step process: (1) the conversion of  $\text{NO}_x$  to nitrite and nitrate and (2) the binding of formed N species with cement paste. The difference in  $\text{NO}_x$  uptake is related to the differences in microstructural features (i.e. SSA and pore size distribution) and the photocatalytic activity induced by  $\text{TiO}_2$  addition. These factors can be examined independently by comparing results among different sample groups.

##### 3.3.1. Effect of microstructural features

For the plain OPC samples that are exposed to  $\text{NO}_x$  (PB-N and PB-N-V), both nitrite and nitrate are detected after exposure. As shown in Table 3, similar amounts of nitrite and nitrate are measured regardless of the presence of UV light. Therefore, the mechanism of converting  $\text{NO}_x$  to nitrite and nitrate by plain OPC is unlikely to be photocatalytic.

The mechanism of  $\text{NO}_x$  conversion to nitrite and nitrate should be related to heterogeneous catalytic reactions on the surface of hydrated cements. Researchers have demonstrated these reactions of  $\text{NO}_x$  on many different hydrated mineral surfaces [48–50]. For example, Grassian showed that  $\text{NO}_x$  reacts on the surface of hydrated  $\text{SiO}_2$  particles (particles exposed to water overnight) but not on dehydrated  $\text{SiO}_2$  particles (particles evacuated overnight) [48]. The detection of nitrite and nitrate in this study suggests that the complex surfaces of hydrated cementitious materials with their monolayers of water and pore-solution containing nanopores can also facilitate these heterogeneous catalytic reactions. Horgnies et al. [51] also observed decreased  $\text{NO}_x$  levels in the presence of conventional plain concrete and suggested that the high alkalinity in the cementitious environment also played an important role in  $\text{NO}_x$  conversion to nitrite and nitrate. Their proposed reactions with hydroxyls are as below:

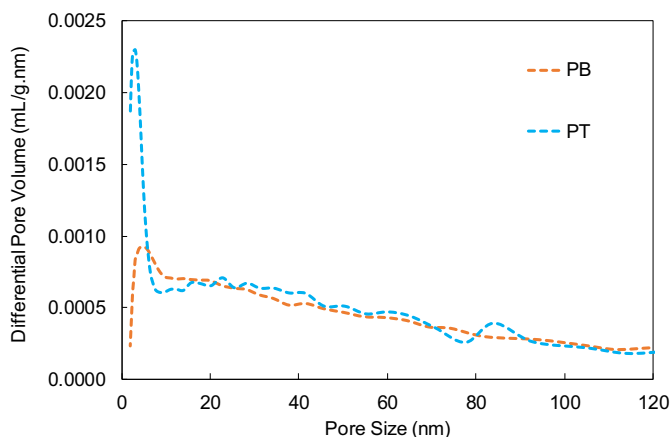
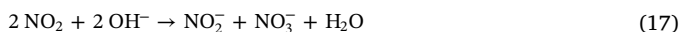
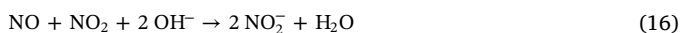


Fig. 2. Pore size distribution of plain OPC (PB) and 5%  $\text{TiO}_2$ -doped OPC (PT) samples.



The previous studies also suggested that the heterogeneous surface catalytic reactions could be accelerated by high surface area, which relates to surface roughness, amount of micropores, and particle size [48–50]. This is also evidenced in this study by examining samples that are only exposed to  $\text{NO}_x$  (PB-N and PT-N), but with different SSA and amount of micropores. For Sample PT-N, the increase in  $\text{NO}_x$  uptake can be associated with the effect of  $\text{TiO}_2$  addition on increased SSA and the amount of micropores with a size of < 5 nm (Section 3.1). Lee et al. [31] have also observed similar results indicating that a greater degree of  $\text{NO}_x$  degradation was achieved in  $\text{TiO}_2$ -doped cement pastes with a larger SSA. They have also suggested that the greater amount of micropores could also help hold more alkaline pore solution, which in turn could accommodate more nitrite and nitrate. Therefore, the  $\text{NO}_x$  uptake can be directly related to the microstructural features of cementitious materials.

Although the above studies have demonstrated the heterogeneous surface catalytic reactions in Sample PB-N and PT-N, none of them quantified the  $\text{NO}_x$  uptake. This information is critical to understand the intrinsic  $\text{NO}_x$  sequestration capability of cementitious materials and can be used it to remediate  $\text{NO}_x$  emissions resulting from their own production. This study quantifies the amount of  $\text{NO}_x$  uptake by measuring the concentration of nitrite and nitrate. The results are listed in Table 3. The concentration of both nitrite and nitrate in Sample PT-N increases compared to PB-N. The total N mass of  $\text{NO}_x$  uptake of PT-N is increased by 65% compared to PB-N. This increase coincides with the increase of SSA measured in Section 3.1. The increase in the nitrite is about 110% while the increase in the nitrate is about 30%. This difference leads to a change of the nitrite:nitrate concentration ratio from 1:2 in Sample PB-N to 1:1.3 in Sample PT-N. As discussed in Section 3.1, the higher SSA and greater amount of micropores in Sample PT-N induced by  $\text{TiO}_2$  addition indicates a greater volume of C-S-H, in addition to the surface area and porosity intrinsic to the  $\text{TiO}_2$  nanoparticles. Therefore, the increase of total  $\text{NO}_x$  uptake and larger increase of nitrite could be related to the increased amount of and more dispersed C-S-H and its different interaction with nitrite and nitrate. Again, the microstructural features, including SSA and pore size distribution, could be used as indicators to design cementitious materials for optimized  $\text{NO}_x$  uptake.

### 3.3.2. Effect of photocatalytic reactions

The total amount of  $\text{NO}_x$  uptake is increased by 360% in  $\text{TiO}_2$ -doped OPC that exposed to  $\text{NO}_x$  and UV light (PT-N-V) compare to the plain OPC samples (PB-N-V). The increased  $\text{NO}_x$  uptake is related to both the microstructural differences and the activation of photocatalytic activities induced by  $\text{TiO}_2$  addition. The effects of microstructural features of cementitious materials on  $\text{NO}_x$  uptake have been discussed in the previous section.

The highest increase in  $\text{NO}_x$  uptake in Sample PT-N-V is mainly due to the photocatalytic activities (Eq. 1–8), which increase the conversion of  $\text{NO}_x$  to nitrite and nitrate ions and subsequently  $\text{NO}_x$  uptake. The relative amounts of nitrite and nitrate from the photocatalytic process alone (i.e., neglecting binding by the cementitious material itself) can also be determined by comparing Samples PT-N and PT-N-V. The results are provided in Table 3. Approximately half of the  $\text{NO}_x$  uptake is converted into nitrite during photocatalytic reactions, and the other half into nitrate. The higher  $\text{NO}_x$  uptake in Sample PT-N-V (360%) compared to Sample PT-N (65%) also indicates that the photocatalytic activity has a greater effect on  $\text{NO}_x$  uptake than the microstructural differences associated with  $\text{TiO}_2$  introduction.

## 4. Conclusions

The  $\text{NO}_x$  uptake for both plain and  $\text{TiO}_2$ -doped OPC samples is

compared in this study. Because  $\text{NO}_x$  is converted to nitrite and nitrate ions on the material surface, a combination of wet chemical extraction, UV–vis spectrophotometry and ion chromatography methods were used to quantify the concentrations of nitrite and nitrate that are bound within the hydrated cement paste. A mass balance is achieved between the total  $\text{NO}_x$  uptake and nitrite and nitrate formation. The effects of microstructural properties and photocatalytic reactions on  $\text{NO}_x$  uptake are examined. The conclusions are given below:

1. Similar  $\text{NO}_x$  uptake is observed in plain OPC samples (PB-N and PB-N-V) regardless of the presence of UV light, demonstrating that cement-based materials have the capacity for  $\text{NO}_x$  sequestration even in the absence of photocatalysts. By confirming the  $\text{NO}_x$  sequestration capability of plain OPC, policy makers can develop new strategies of remediating atmospheric  $\text{NO}_x$  by taking advantage of the  $\text{NO}_x$  sequestration capability of existing cement-based infrastructure, such as using it to remediate  $\text{NO}_x$  emissions resulting from their own production and construction.
2. The mechanism of  $\text{NO}_x$  conversion into nitrite and nitrate in samples that are only exposed to  $\text{NO}_x$  (PB-N and PT-N) is related to the surface catalytic reactions in cementitious environment. The addition of  $\text{TiO}_2$  nanoparticles enhanced cement hydration and formation of C-S-H via nucleation and growth effects. The greater amount of C-S-H and the nano- $\text{TiO}_2$  addition contribute to the increase in SSA and the amount of < 5 nm micropores, and in turn increase the potential for  $\text{NO}_x$  uptake. The alkalinity in cementitious environment also plays an important role in  $\text{NO}_x$  conversion. With the  $\text{TiO}_2$  addition, the concentration ratio between nitrite and nitrate changes from 1:2 to 1:1.3. This change is likely due to the larger amount of C-S-H in  $\text{TiO}_2$ -doped OPC samples. Therefore, the microstructural features, including SSA and pore size distribution, can be used as indicators for designing cementitious materials for optimized  $\text{NO}_x$  uptake.
3. For  $\text{TiO}_2$ -doped OPC samples that are exposed to both  $\text{NO}_x$  and UV (PT-N-V), the total  $\text{NO}_x$  uptake increases by 360%, compared to the plain OPC sample under the same exposure conditions (PB-N-V). The increase is attributed to the microstructure differences and activation of photocatalytic reactions induced by  $\text{TiO}_2$  nanoparticles. By comparing the  $\text{TiO}_2$ -doped OPC samples with and without UV light exposure (PT-N-V vs PT-N), it can be concluded that the  $\text{NO}_x$  uptake is more greatly influenced by the photocatalytic activity than the microstructural changes associated with  $\text{TiO}_2$  introduction.

## Acknowledgements

This work is supported by the National Science Foundation under Grant No. CMMI-1362843. Any opinions, findings, and conclusions or recommendations expressed in this material are those of the author(s) and do not necessarily reflect the views of the National Science Foundation.

## References

- [1] R.M. Harrison *Pollution, Causes, Effects and Control*, 2 the Royal Society of Chemistry, Cambridge, (1992).
- [2] The U.S. Environmental Protection Emission Standards for Electric Standards “United States Office of Air Quality Planning and Standards EPA-456/F-98-005”, Protection Research Triangle Park, NC 27711, (September 1998).
- [3] D. Elsom, *Atmospheric Pollution*, vol. 1, Basil Blackwell, New York, 1987.
- [4] J.H. Seinfeld, *Atmospheric Chemistry and Physics: From Air Pollution to Climate Change*, vol. 1, Wiley, New York, 1998.
- [5] Primary National Ambient air Quality Standards for Nitrogen Dioxide; Final Rule, 75 Fed. Reg. 26, (February 9, 2010) (to be codified at 40 C.F.R. pts. 50, 58).
- [6] C.A. Latta, R.F. Weston, *Methods for Reducing NOx Emissions*, Plant Engineering, (1998) (September 1998).
- [7] A. Fujishima, K. Honda, Electrochemical photolysis of water at a semiconductor electrode, *Nature* 238 (1972) 37–38.
- [8] A. Fujishima, K. Hashimoto, T. Watanabe, *TiO2 Photocatalysis: Fundamentals and Applications*, BKC Inc, Tokyo, 1999.

- [9] M.M. Ballari, Q.L. Yu, H.J.H. Brouwers, Experimental study of the NO and NO<sub>2</sub> degradation by photocatalytically active concrete, *Catal. Today* 161 (2011) 175–180.
- [10] R. Sugrañez, J.I. Alvarez, M. Cruz-Yusta, I. Marmol, J. Morales, J. Vila, L. Sanchez, Enhanced photocatalytic degradation of NO<sub>x</sub> gases by regulating the microstructure of mortar cement modified with titanium dioxide, *Build. Environ.* 69 (2013) 55–63.
- [11] M.M. Ballari, H.J.H. Brouwers, Full scale demonstration of air-purifying pavement, *J. Hazard. Mater.* 254 (2013) 406–414.
- [12] M.M. Hassan, H. Dylla, L.N. Mohammad, T. Rupnow, Evaluation of the durability of titanium dioxide photocatalyst coating for concrete pavement, *Cons. Build. Mater.* 24 (2010) 1456–1461.
- [13] C.S. Poon, E. Cheung, NO removal efficiency of photocatalytic paving blocks prepared with recycled materials, *Const. Build. Mater.* 21 (2007) 1746–1753.
- [14] A. Folli, S.B. Campbell, J.A. Anderson, D.E. Macphee, Role of TiO<sub>2</sub> surface hydration on NO oxidation photo-activity, *J. Photochem. Photobiol. A Chem.* 220 (2011) 85–93.
- [15] M. Montes, F.P. Getton, M.S.W. Vong, P.A. Sermon, Titania on silica. A comparison of sol-gel routes and traditional methods, *J. Sol-Gel Sci. Technol.* 8 (1997) 131–137.
- [16] A.M. Ramirez, K. Demeestere, N. De Belie, T. Mäntylä, E. Levänen, Titanium dioxide coated cementitious materials for air purifying purposes: preparation, characterization and toluene removal potential, *Build. Environ.* 45 (2010) 832–838.
- [17] J.S. Dalton, P.A. Janes, N.G. Jones, J.A. Nicholson, K.R. Hallam, G.C. Allen, Photocatalytic oxidation of NO<sub>x</sub> gases using TiO<sub>2</sub>: a surface spectroscopic approach, *Environ. Pollut.* 120 (2002) 415–422.
- [18] M.M. Ballari, M. Hunger, G. Hüsken, H.J.H. Brouwers, NO<sub>x</sub> photocatalytic degradation employing concrete pavement containing titanium dioxide, *Appl. Catal. B Environ.* 95 (2010) 245–254.
- [19] R. Sugrañez, J.I. Álvarez, M. Cruz-Yusta, I. Marmol, J. Morales, J. Vila, L. Sánchez, Enhanced photocatalytic degradation of NO<sub>x</sub> gases by regulating the microstructure of mortar cement modified with titanium dioxide, *Build. Environ.* 69 (2013) 55–63.
- [20] J. Chen, C.S. Poon, Photocatalytic cementitious materials: influence of the microstructure of cement paste on photocatalytic pollution degradation, *Environ. Sci. Technol.* 43 (2009) 8948–8952.
- [21] A. Yousefi, A. Allahverdi, P. Hejazi, Effective dispersion of nano-TiO<sub>2</sub> powder for enhancement of photocatalytic properties in cement mixes, *Constr. Build. Mater.* 41 (2013) 224–230.
- [22] Q.L. Yu, H.J.H. Brouwers, Indoor air purification using heterogeneous photocatalytic oxidation. Part I: experimental study, *Appl. Catal. B Environ.* 92 (2009) 454–461.
- [23] M.Z. Guo, A. Maury-Ramirez, C.S. Poon, Photocatalytic activities of titanium dioxide incorporated architectural mortars: effects of weathering and activation light, *Build. Environ.* 94 (2015) 395–402.
- [24] M. Pérez-Nicolás, J. Balbuena, M. Cruz-Yusta, L. Sánchez, I. Navarro-Blasco, J.M. Fernández, J.I. Alvarez, *Cem. Concr. Res.* 70 (2015) 67–76.
- [25] Baoguo Ma, Hainan Li, Xiangguo Li, Junpeng Mei, Yang Lv, Influence of nano-TiO<sub>2</sub> on physical and hydration characteristics of fly ash–cement systems, *Constr. Build. Mater.* 122 (2016) 242–253.
- [26] J. Chen, C.S. Poon, Photocatalytic construction and building materials: from fundamentals to applications, *Build. Environ.* 44 (2009) 1899–1906.
- [27] G. Hüsken, M. Hunger, H.J.H. Brouwers, Experimental study of photocatalytic concrete products for air purification, *Build. Environ.* 44 (2009) 2463–2474.
- [28] D.E. Macphee, A. Folli, Photocatalytic concretes — the interface between photocatalysis and cement chemistry, *Cem. Concr. Res.* 85 (2016) 48–54.
- [29] M.M. Ballari, Q.L. Yu, H.J.H. Brouwers, Experimental study of the NO and NO<sub>2</sub> degradation by photocatalytically active concrete, *Catal. Today* 161 (1) (2011) 175–180.
- [30] S. Devahasdin, C.J. Fan, K. Li, D.H. Chen, TiO<sub>2</sub> photocatalytic oxidation of nitric oxide: transient behavior and reaction kinetics, *J. Photochem. Photobiol. A Chem.* 156 (2003) 161–170.
- [31] B.Y. Lee, A.R. Jayapalan, M.H. Bergin, K.E. Kurtis, Photocatalytic cement exposed to nitrogen oxides: effect of oxidation and binding, *Cem. Concr. Res.* 60 (2014) 30–36.
- [32] M. Balonis, M. Medala, F.P. Glasser, Influence of calcium nitrate and nitrite on the constitution of AFm and AFt cement hydrates, *Adv. Cem. Res.* 23 (3) (2011) 129–143.
- [33] H. Justnes, Corrosion inhibitors for reinforced concrete, *Corros. Reinf. Concr. Struct.* (2005) 190–214.
- [34] G. Falzone, M. Balonis, D. Bentz, S. Jones, G. Sant, Anion capture and exchange by functional coatings: new routes to mitigate steel corrosion in concrete infrastructure, *Cem. Concr. Res.* 101 (2017) 82–92.
- [35] K.M. Miranda, M.G. Espey, D.A. Wink, A rapid, simple spectrophotometric method for simultaneous detection of nitrate and nitrite, *Nitric Oxide* 5 (1) (2001) 62–71.
- [36] Q.H. Wang, L.J. Yu, Y. Liu, L. Lin, R.G. Lu, J.P. Zhu, Z.L. Lu, Methods for the detection and determination of nitrite and nitrate: a review, *Talanta* 165 (2017) 709–720.
- [37] ASTM, Standard C114, "Standard Test Methods for Chemical Analysis of Hydraulic Cement", ASTM International, West Conshohocken, PA, 2013, <https://doi.org/10.1520/C0114-13>.
- [38] S. Brunauer, P.H. Emmett, E. Teller, Adsorption of gases in multimolecular layers, *J. Am. Chem. Soc.* 60 (2) (1938) 309–319.
- [39] E.P. Barrett, L.G. Joyner, P.P. Halenda, The determination of pore volume and area distributions in porous substances. I. Computations from nitrogen isotherms, *J. Am. Chem. Soc.* 73 (1) (1951) 373–380.
- [40] M. Palacios, H. Kazemi-Kamyab, S. Mantellato, P. Bowen, Laser diffraction and gas adsorption techniques, in: K. Scrivener, R. Snellings, B. Lothenbach (Eds.), *A Practical Guide to Microstructural Analysis of Cementitious Materials*, CRC Press, 2015, pp. 445–484.
- [41] I. Odler, The BET-specific surface area of hydrated Portland cement and related materials, *Cem. Concr. Res.* 33 (12) (2003) 2049–2056.
- [42] M.C.G. Juenger, H.M. Jennings, The use of nitrogen adsorption to assess the microstructure of cement paste, *Cem. Concr. Res.* 31 (6) (2001) 883–892.
- [43] ISO Fine Ceramics (Advanced Ceramics, Advanced Technical Ceramics) - Test Method for Air-Purification Performance of Semiconducting Photocatalytic Materials Part 1: Removal of Nitric Oxide, (2007).
- [44] JIS R 1701-1 Fine Ceramics (Advanced Ceramics, Advanced Technical Ceramics) - Test Method for Air Purification Performance of Photocatalytic Materials-Part 1: Removal of Nitric Oxide, Japanese Standards Association, Tokyo, Japan, 2004.
- [45] A. Jayapalan, B. Lee, S. Fredrich, K. Kurtis, Influence of additions of anatase TiO<sub>2</sub> nanoparticles on early-age properties of cement-based materials, *Transportation Research Record: Journal of the Transportation Research Board* 2141 (2010) 41–46.
- [46] B.Y. Lee, K.E. Kurtis, Influence of TiO<sub>2</sub> nanoparticles on early C3S hydration, *J. Am. Ceram. Soc.* 93 (10) (2010) 3399–3405.
- [47] J.J. Thomas, H.M. Jennings, A.J. Allen, The surface area of cement paste as measured by neutron scattering: evidence for two C-S-H morphologies, *Cem. Concr. Res.* 28 (6) (1998) 897–905.
- [48] V.H. Grassian, Chemical reactions of nitrogen oxides on the surface of oxide, carbonate, soot, and mineral dust particles: implications for the chemical balance of the troposphere, *J. Phys. Chem. A* 106 (6) (2002) 860–877.
- [49] A. Febo, C. Perrino, Prediction and experimental evidence for high air concentration of nitrous acid in indoor environments, *Atmos. Environ. Part A* 25 (5–6) (1991) 1055–1061.
- [50] M.E. Jenkin, R.A. Cox, D.J. Williams, Laboratory studies of the kinetics of formation of nitrous acid from the thermal reaction of nitrogen dioxide and water vapour, *Atmospheric Environment* (1967) 22 (3) (1988) 487–498.
- [51] M. Horgnies, I. Dubois-Brugger, E.M. Gartner, NO<sub>x</sub> de-pollution by hardened concrete and the influence of activated charcoal additions, *Cem. Concr. Res.* 42 (2012) 1348–1355.